Available online at www.sciencedirect.com
SCIENCE DIRECT®
Journal of Hydrology xx (2005) 1–21
Journal of Hydrology
www.elsevier.com/locate/jhydrol

Repeated surveys by acoustic Doppler current profiler for flow and sediment dynamics in a tidal river

R.L. Dinehart*, J.R. Burau

US Geological Survey, 6000 J Street, Placer Hall, Sacramento, CA 95819, USA

Received 9 February 2004; revised 8 February 2005; accepted 7 March 2005

Abstract

A strategy of repeated surveys by acoustic Doppler current profiler (ADCP) was applied in a tidal river to map velocity vectors and suspended-sediment indicators. The Sacramento River at the junction with the Delta Cross Channel at Walnut Grove, California, was surveyed over several tidal cycles in the Fall of 2000 and 2001 with a vessel-mounted ADCP. Velocity profiles were recorded along flow-defining survey paths, with surveys repeated every 27 min through a diurnal tidal cycle. Velocity vectors along each survey path were interpolated to a three-dimensional Cartesian grid that conformed to local bathymetry. A separate array of vectors was interpolated onto a grid from each survey. By displaying interpolated vector grids sequentially with computer animation, flow dynamics of the reach could be studied in three-dimensions as flow responded to the tidal cycle. Velocity streamtraces in the grid showed the upwelling of flow from the bottom of the Sacramento River channel into the Delta Cross Channel. The sequential display of vector grids showed that water in the canal briefly returned into the Sacramento River after peak flood tides, which had not been known previously.

In addition to velocity vectors, ADCP data were processed to derive channel bathymetry and a spatial indicator for suspended-sediment concentration. Individual beam distances to bed, recorded by the ADCP, were transformed to yield bathymetry accurate enough to resolve small bedforms within the study reach. While recording velocity, ADCPs also record the intensity of acoustic backscatter from particles suspended in the flow. Sequential surveys of backscatter intensity were interpolated to grids and animated to indicate the spatial movement of suspended sediment through the study reach. Calculation of backscatter flux through cross-sectional grids provided a first step for computation of suspended-sediment discharge, the second step being a calibrated relation between backscatter intensity and sediment concentration. Spatial analyses of ADCP data showed that a strategy of repeated surveys and flow-field interpolation has the potential to simplify computation of flow and sediment discharge through complex waterways.

The use of trade, product, industry, or firm names in this report is for descriptive purposes only and does not constitute endorsement of products by the US Government.

Keywords: ADCP; Velocity; Backscatter intensity; Suspended sediment; Tidal river

* Corresponding author. Tel.: +1 916 278 3175; fax: +1 916 278 3071.
E-mail address: rldine@usgs.gov (R.L. Dinehart).

0022-1694/$ - see front matter © 2005 Elsevier B.V. All rights reserved.
doi:10.1016/j.jhydrol.2005.03.019

1. Introduction

In surface-water hydrology, acoustic Doppler current profilers (ADCPs) are especially useful for measuring stream discharge rapidly in large rivers with unsteady flows (Simpson and Oltmann, 1993). The velocity-vector components recorded by vessel-mounted ADCPs can be plotted at precise geographic coordinates recorded by Global Positioning System (GPS). This capability was exploited to map velocity vectors in a reach of the Sacramento River as part of a study by the US Geological Survey (USGS) with fisheries-management agencies. Time-based visualizations of flow and sediment dynamics in this tidal river were derived from sequences of ADCP data surveys. The purpose of this paper is to describe the methods and benefits of mapping ADCP data obtained within a channel junction affected by tidal fluctuations.

A reach of the Sacramento River was surveyed repeatedly in 2000 and 2001 by vessel-mounted ADCPs along flow-defining paths at a junction with a diversion canal, known as Delta Cross Channel. Each circuit around a survey path in the junction, called an 'ADCP survey,' produced several hundred vertical profiles of velocity, distributed across the channel and in the canal entrance. The ADCP surveys were intended to document flow dynamics associated with fish migration past the canal entrance. Spatial analyses of the ADCP data (Dinehart, 2003) indicated changes in flow fields and sediment distributions from one ADCP survey to the next. This article describes procedures for mapping velocity, bathymetry, and backscatter intensity from ADCP data to a three-dimensional volume, using as a case study the surveys near the Delta Cross Channel (the 'canal'). Through this example, we demonstrate an adaptable strategy to derive interpolated flow-field grids of velocity and backscatter intensity from repeated ADCP surveys. Then, we examine the flow and sediment dynamics at the junction derived from sequences of interpolated grids of velocity and backscatter intensity.

Three-dimensional velocities have been measured in natural open channels more completely with advances in flow instrumentation (Nezu et al., 1993; Sukhodolov et al., 1998; Lane et al., 1998). The flow fields of river-channel junctions have been studied extensively for engineering purposes and geomorphological research. Many 3D velocity surveys at channel junctions describe confluent flows from lesser tributaries (Rhoads and Kenworthy, 1995; De Serres et al., 1999). The study in the Sacramento River at Delta Cross Channel examined difluent flow from a large tidal river into a smaller distributary. Although velocity in the junction was surveyed as ancillary data for the fisheries study, the new procedures developed there provided a case study for spatial mapping of velocity with commercial ADCPs in tidal river flows.

The large number of ADCP surveys made in this study, over 60 in each of several 24 h periods, provided far greater detail on flow properties for this site than was available previously. Each ADCP survey was completed in about 27 min. The channel area covered by each ADCP survey was about 100 m (across the channel) by 300 m (along the channel). By repeating travel along the survey path frequently, velocity could be sampled throughout the flow field as it changed during the diurnal tidal cycle (24.48 h). As shown later, tidal stage and velocity changed minimally during each ADCP survey. Given the unsteady flow condition, a quasi-synoptic measurement was still assumed for each ADCP survey, in the sense that all data acquired in a survey were treated as if collected at an identical time.

Interpolation of sparse flow-field data to regular grids is essential in spatial velocity surveys for oceanographic studies (Matthews, 1997). In surface-water hydrology, techniques to map flow fields in open channels are not used routinely and are not widely tested. We interpolated ADCP velocities to grids to map flow-field directions with limited data acquisition over a wide reach. By assuming synopticity of the ADCP velocity measurements, we consequently assumed that sequences of interpolated grids indicated the flow dynamics in the study reach.

Flow dynamics refers to changes in flow properties derivable from sequences of velocity surveys. Similarly, sediment dynamics can be considered the collective changes in sediment concentration, distribution, and movement accompanying the tidal flow. While recording velocity, ADCPs also record the acoustic intensity of signals backscattered to the device from particles suspended in the flow. Sequential surveys of backscatter intensity were interpolated to grids and animated to indicate the movement of

suspended sediment through the study reach. Calibration of sediment concentration from ADCP data deserves fuller discussion, and is not included in our exposition of survey strategies. We present only the processed backscatter data, rather than a preferred method of conversion from backscatter intensity to sediment concentration.

2. Study reach and goals

Flow conditions were surveyed in a 0.3-km reach of the lower Sacramento River, midway along a bend with a radius of curvature of about 0.9 km, near the west entrance to the Delta Cross Channel (Fig. 1). The canal entrance is situated at the outside of the bend at Walnut Grove, California. Swing gates allow river water into the canal when they are opened. At designated times, the canal diverts water from the lower Sacramento River to the middle reaches of San Joaquin River by passage through the intermediary Mokelumne River. In the study reach upstream from the canal entrance, river flow does not reverse direction significantly. Although river flow is directed seaward throughout most of the tidal cycle, velocities near the canal entrance approach zero at the slack of each flood tide. As stage rises, river flow is diverted into the canal. Flow into the canal entrance decreases as ebb tide begins, and after maximum ebb, stage rises and water again enters the canal. However, tidal stage in the Sacramento River is not the sole determinant of flow into the canal entrance. Instead, a phase lag of water-surface slope between the Sacramento and Mokelumne Rivers controls the timing of flow diversion into the canal.

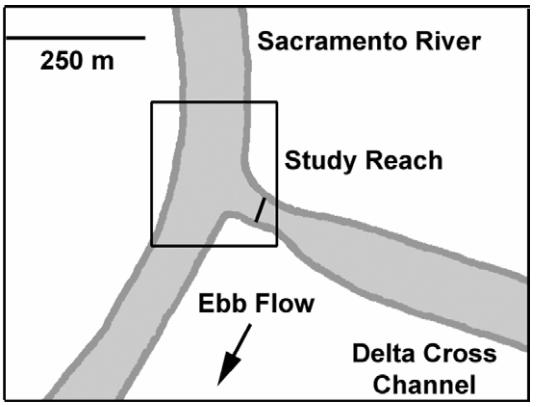

Fig. 1. Diagram of study reach for Sacramento River at Delta Cross Channel near Walnut Grove, California.

In the fall, natural and regulated flows in watersheds of the Central Valley recede to low-levels, putting surface-water supplies at risk of contamination by salt water intrusion from eastern San Francisco Bay. At those times, additional flow is diverted from the Sacramento River into the Delta Cross Channel primarily to maintain fresh water in the lower San Joaquin River and its tributaries. However, the flow diversions are often made during seasonal salmon runs, thereby risking the loss of salmon smolt by detours from their natural migratory routes.

Investigations into smolt migration near the Delta Cross Channel have been described by US Fish and Wildlife Service (1992), Hanson (1996), and Kjelson et al. (1999). Their common finding was that smolts are drawn into the canal during flood tide, sending them away from their seaward routes, and directing them to the interior of the San Joaquin River Delta. Fisheries researchers have recognized the potential for loss of salmon smolts in tributaries of the San Joaquin River, at pump intakes used for intra-state transfer of water. Biologists developed an experiment to determine the proportion of salmon smolts diverted from the main channel during various flows into the Delta Cross Channel (Horn, 2003). As part of this study, one of the authors (Burau) designed routes to be mapped with the ADCP data by methods previously developed by the other author (Dinehart, 2000). Velocity mapping was scheduled to observe the effects of flow diversion on the release of salmon smolt during migration in Falls 2000 and 2001 (Burau et al., 2003a). This goal of velocity mapping was attained through application of the methods described below.

3. Channel-surveying methods

The study reach was surveyed by vessel-mounted ADCPs connected to GPS receivers. Broadband ADCPs (RD Instruments, San Diego) were used in the repeated surveys to map velocity vectors and channel bathymetry in the study reach. The ability to incorporate GPS data with ADCP discharge measurements was developed in 1998, and GPS logging was included with Windows-based software used in

Table 1
Number and duration of representative ADCP surveys during two campaigns at Sacramento River at Walnut Grove, with associated flow conditions

Survey campaign	Start	Finish	Number of surveys	Average time between mid-survey times, in minutes	Tidal range, in meters	Time between ensembles, in seconds	Mean discharge, in m^3/s
Fall 2000	15:55 Nov. 13	21:31 Nov. 14	66	27	0.9	4.4	212
	15:42 Nov. 20	20:40 Nov. 21	65	27	0.8	4.4	241
Fall 2001	6:18 Oct. 29	11:39 Oct. 30	63	28	0.6	1.9	164
	7:14 Nov. 1	11:01 Nov. 2	63	26	0.9	1.9	198

the surveys (*WinRiver*, v. 10.03, RD Instruments). For this study, a 1200-Hz ADCP was used to measure velocity while mounted on the side of a 7-m, fiberglass-hull boat, and was connected with a differential GPS receiver to provide navigational positions. The number, duration, and parameters of ADCP surveys during two representative survey episodes are given in Table 1. The survey campaigns of November 9–20, 2000, and October 29–November 2, 2001, are termed the Falls 2000 and 2001 surveys, respectively.

Water velocity in the study reach was measured with ADCPs using techniques described by Gordon (1996), which are summarized here. Pulse-coded sonar signals are transmitted along four beams from the ADCP and then scattered and reflected from moving particles back to the transducers. The transmitted frequency is compared with the frequency received along each beam. The differences in frequency constitute a Doppler shift that is combined with vessel speed and heading to derive a water-velocity magnitude and bearing. As the ADCP moves with a vessel, the device records velocity vectors at multiple elevations simultaneously for the range of depth. The set of velocity vectors at each lateral position is a 'velocity ensemble.' The ADCP also uses sonar to track vessel movement over the streambed, with an internal feature called 'bottom-tracking.' Absolute vessel speed is determined by reference to the streambed, using an internal compass and the bottom-tracking feature.

The velocity-mapping strategy benefited from the familiarity with ADCP operations gained here by local USGS researchers. A calculation system for discharge measurement from ADCP data was developed with testing on the Sacramento River by Simpson and Oltmann (1993). Improved techniques of discharge measurement by ADCPs have been developed by extended testing and analysis in the channels of the Sacramento River Delta (Simpson and Bland, 2000). Physical operation of the ADCP for discharge measurements has been described in detail by Simpson (2001). With this experience, the measuring crews quickly adapted existing ADCPs and techniques to the velocity-mapping strategy.

The time duration of each ADCP survey was made brief enough that the series of surveys would resolve short-term changes in the flow field across the Sacramento River channel. Because the vessel obviously cannot be at all points of the reach simultaneously, flow-defining survey paths were designed to minimize the time of each circuit while maximizing flow-field definition. The choice of duration time was guided by the total range of tidal stage (about 1 m or less) and the time from maximum flood to maximum ebb (about 8 h). A survey path was chosen that could be traveled in 20–30 min, with a delay of 5 min or less between circuits. For the duration of an ADCP survey, the change in stage was less than 10 cm, and the corresponding change in mean velocity was 10 cm/s or less. Each ADCP survey contained from 500 to 1000 velocity ensembles distributed along the survey path. In practice, between 15 and 18 ADCP surveys were made during an 8-h period from maximum flood to maximum ebb.

The survey paths were chosen to suit the study goal of resolving the flow field synoptically, over time. In the Fall 2000 surveys, paths were oriented along main-channel streamlines (Fig. 2A). To define the flow field, six longitudinal profiles were traced in rectangular loops along the main channel, beginning

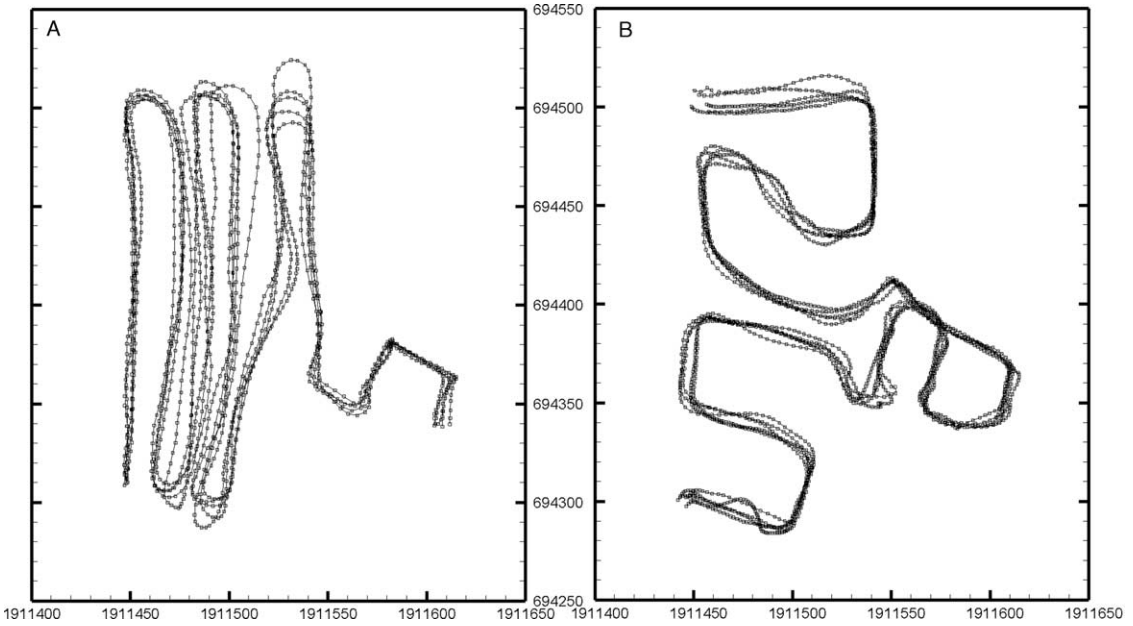

Fig. 2. Five typical survey paths with GPS positions for Fall 2000 (A) and Fall 2001 (B).

at the right bank. After the vessel crossed the canal entrance, it traveled along the canal bank, crossed the canal once, traveled along the opposite bank, and crossed once more, ending the ADCP survey. However, examination of the velocity ensembles from the Fall 2000 surveys showed that the flow field near the canal entrance was not well defined. A possible time bias in velocity measurement was also created by surveying the canal entrance after the main channel was surveyed.

To better define streamline vectors, paths of the Fall 2001 surveys were reoriented to cross the main channel at six sections and the canal entrance at three sections (Fig. 2B). The crossings were made in curved loops near the canal entrance, so that survey paths were more perpendicular to prevailing streamlines. The canal was entered by the vessel halfway through the ADCP survey, which decreased the possible time bias.

The ADCP settings were chosen to improve measurement of velocity ensembles near the canal entrance. Each velocity of an ensemble was measured at one of multiple 'bins' (vertical ranges) with center-to-center distances between bins of 0.25 m. Mean depth of the Delta Cross Channel near the entrance was 5 m, and the deepest section of the main channel exceeded 14 m. Therefore, the number of bins containing measured velocities in the vertical ranged from 15 to 50. Typical ADCP practice is to leave the nearest 0.5 m beneath the transducer unmeasured, due to acoustic limitations. The ADCP was set to average five ensembles internally before transmitting the resulting ensemble (Gordon, 1996). This setting increases the time between acquisition of each ensemble, but reduces the standard deviation of vectors. During the Fall 2000 surveys, velocity ensembles were acquired and transmitted every 4.4 s. This rate, combined with a vessel speed of 1–1.5 m/s, yielded point-to-point distances near an average of 5 m along survey paths. With improved computer hardware, the data-transmission rate was increased during the Fall 2001 surveys, which reduced the acquisition rate for velocity ensembles to 1.9 s, and reduced the average point-to-point distance to less than 2 m.

4. Data-processing methods

Data-processing methods and corrections applied to extracted ADCP data are described here, followed by a description of interpolation procedures for

velocity and backscatter intensity. Data files acquired by the ADCP were output from *WinRiver* in text form, with a separate file for each survey path. Two commercial software programs were used together to extract and view data in files output from *WinRiver*. Program algorithms for processing ADCP data were written in *Microsoft Excel with Visual Basic for Applications*. Graphical procedures for spatial analysis and display of ADCP data were designed using *Tecplot*, a 3D flow visualization program by Tecplot, Inc.

With nearly 60 ADCP surveys acquired per diurnal tidal cycle, the manual preparation of thousands of velocity ensembles for visualization became time consuming. To automate the data processing, a collection of routines was created in *Visual Basic for Applications*. The routines were used to register vector components to geographic coordinates and local river datum, filter velocity ensembles by removing outlier values, vertically average the filtered ensembles, extract backscatter values, and prepare data files for inclusion in plotting programs (Dinehart, 2003). Subsets of ADCP data (e.g. navigational positions, bathymetric data, velocity ensembles, backscatter intensity) were extracted from multiple surveys using batch processing. Most subsets were then adjusted automatically or by user intervention. Necessary corrections were applied as described below.

4.1. Navigational positions

The GPS positions are recorded in latitude–longitude coordinates of the World Geographic System, 1984 (WGS84), and were applied as the positional record for ADCP surveys to allow spatial mapping. In spite of the cumulative error documented in bottom-tracking position, velocities were referenced to the vessel speed as determined by bottom tracking. This choice was made because vessel speed calculated from bottom tracking varies less than vessel speed calculated from GPS position, yielding more consistent velocity vectors along survey paths.

Reception of GPS signals near the Delta Cross Channel was affected occasionally by interference from local broadcast towers. More often, GPS reception in the canal entrance was disrupted or lost as the vessel passed beneath the highway bridge over the canal. A position-correcting algorithm was applied to correct corrupted sections of GPS navigational records with the bottom-tracking record. To apply the algorithm, all GPS positions of a survey path were first plotted for the user to identify corrupted sections. The user would select reliable start and end points that enclosed the corrupted sections. The algorithm then replaced the intervening positions with bottom-track positions that had been offset to match the GPS starting point. Deviations between bottom-track paths and GPS navigational paths are unavoidable, and are caused by a combination of compass-heading errors and distance errors in bottom tracking. These deviations required an incremental correction applied to each bottom-track position in order to match the GPS ending point. This incremental correction was included in the position-correcting algorithm so that the interpolated sequence of positions closely matched the original survey path.

4.2. Bathymetric data

Channel bathymetry was mapped with the ADCP using distances measured along four transducer beams to the bed. Each beam distance is converted internally to a vertical depth, and the four depths are recorded and averaged by the ADCP to give a single depth beneath the device. However, the beam distances are accurate enough to construct reliable bathymetry, by determining the coordinates of each beam contact relative to the ADCP position. The four transducer beams of the ADCP are oriented downward at 20° from vertical. Two of the beams are aligned at 20° from the vertical to port and starboard, while two other beams are aligned at the same angles to fore and aft. The cone angle of each beam is 2°, assuring a small footprint for the beam contact at the river bed. The nominal coordinates of each beam contact are rotated by the pitch and roll readings of the ADCP to their true coordinates.

ADCP depths were transformed to bed elevations at geographic coordinates through algorithms first developed by David Mueller and Ed Fisher of USGS (written commun., 2002), with alternative coordinate rotations by Dinehart (Appendix). Using the navigational record, the rotated $X-Y$ positions of each beam contact relative to the ADCP were translated to geographic coordinates. The Z positions of rotated

beam distances were converted to bed elevation by subtraction from the water-surface elevation corresponding to the mean time of an ADCP survey. The algorithms for coordinate rotations were incorporated into the processing routines developed for repeated ADCP surveys (Dinehart, 2003).

At the study reach, the water-surface elevation used as reference for the ADCP elevation was recorded as river stage at a gaging station near the Delta Cross Channel, (Sacramento River above Walnut Grove, California, Station No. 11447890) operated by the USGS. Between the gaging station and the study reach about 1 km downstream, slope was 1 cm/km, so the recorded stage was applied as the water-surface elevation. A correction of 20 m was added to the recorded stage to retain positive numbers in the z-axis of bathymetric illustrations.

Although a single ADCP survey was insufficient to define channel bathymetry, the large number of bed-elevation points accumulated over multiple survey paths gave sufficient coverage to define a bathymetric surface. Each survey path was offset from a previous path, usually by chance, which generated a distribution of several thousand bed-elevation points throughout the reach (Fig. 3A). The points were interpolated to a regular 2D grid to create a bathymetric surface (Fig. 3B), with grid nodes spaced at 1 m intervals. Accuracy of the survey method was confirmed when small bed features were mapped in deep water at consistent locations, using ADCP surveys made at different tidal stages.

When interpolated bathymetry was examined, systematic errors in the mapping process became apparent. They originated with: minor changes in transducer draft during vessel operation; the uncertainty in measured beam distances; the GPS position of the ADCP; the measured pitch and roll; and the record of water-surface elevation applied at the surveyed reach. These errors combined to produce local deviations up to 0.1 m in both elevation and in horizontal position. Systematic errors in bathymetric mapping were similar in scale to the material

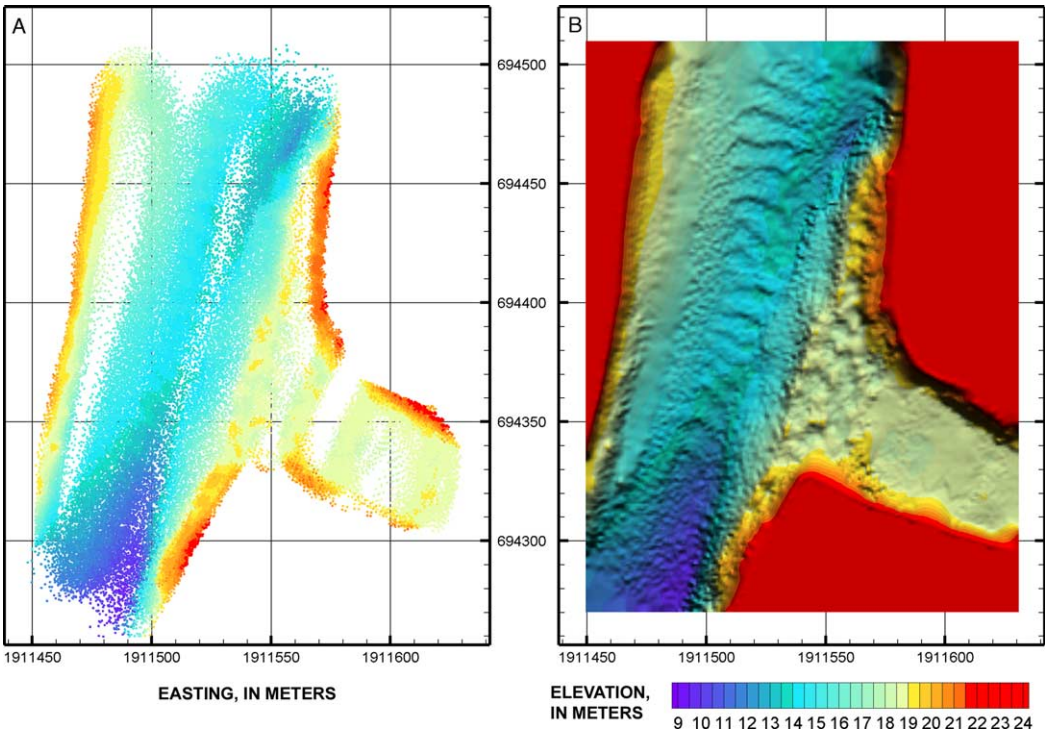

Fig. 3. Bathymetry for junction of Sacramento River at Delta Cross Channel, Fall 2000 surveys. Bed-elevation points from 60 ADCP surveys (A) were interpolated to create a bathymetric grid (B). Bank profiles were interpolated between bed-elevation points and surface planes positioned at the maximum bed elevation. The elevation scale refers to National Geodetic Vertical Datum of 1983, with 20 m added.

composing some riverbeds (small cobbles). If more accurate devices for bathymetric measurement are not available, one can pursue reduction of these errors. Random errors in bed-elevation series were detected as local spikes or zeroes in processing and were corrected manually by inspection.

The Sacramento River channel was profiled longitudinally in the Fall 2000 surveys, yielding accurate definition of sand bedforms (<1.0 m height) approaching the canal entrance (Fig. 3B). The same bedforms were surveyed on four separate episodes during November 2000, and were determined to be stationary during that time. However, the bedforms were not even noticed until the application of the new bathymetric techniques to ADCP depth data. The Fall 2001 surveys did not define bedforms as well, because survey paths crossed bedforms obliquely in the main channel.

4.3. Velocity ensembles

As used in ADCP measurement, the term 'velocity ensemble' indicates a vertical set of velocity vectors at each lateral position. 'Ensemble' indicates only the collection of all velocities at one sampling time, not the statistical sense of a collection of records. Variability was evident in vertical distributions of velocity at all points of the study reach. Near the channel center, horizontal vectors of velocity ensembles covered a range of 30° or more. Vector directions were more variable in ensembles of slower velocities. Near the banks or in slack water, the vectors ranged randomly in all directions. Velocity vectors in ensembles were dominated by macroscale turbulence, and often showed flow deflection past irregular bed topography. The random error of velocity measured in ensembles can be attributed to internal factors such as bin size, ensemble averaging, ambiguity errors, and beam geometry, and to external factors such as ADCP motion (Gordon, 1996). Therefore, velocity ensembles often contain velocities to be disregarded as outliers, especially near the streambed. Several filtering procedures were applied to remove outlier velocities and optionally smooth the profiles, to improve spatial interpolation of flow directions.

The ADCP software program *WinRiver* applies validity checks to velocity data for calculation of discharge at each bin. In processing, velocities were only extracted over the range of bins containing valid discharges, which minimized the extraction of near-bed outliers. The extracted set of u, v, w vector components for each ensemble was registered to geographic coordinates, with each bin elevation referred to local vertical datum by way of stage records. After extraction and registration, velocity ensembles were inspected and filtered so that the spatial interpolation from the ensembles would produce smoother vector grids.

The first pass for filtering removed empty ensembles that were easily identified by a full set of null values, although their origin was unidentified. A second pass removed additional outliers at the bottom of each ensemble, which were usually attributed to ambiguity errors (Gordon, 1996). High velocities near the bed often indicate an ambiguity in the phase measurement for velocity, and produce an opposing vector direction of unrealistic magnitude which is not correctable after acquisition (Gordon, 1996). The bottom value of each ensemble was examined for vector components greatly exceeding the mean; if any component did so, all components at that bin were set to null.

A third, optional pass was used to narrowly smooth the remaining components of velocity ensembles, performing the only numerical changes to original velocity data. Any component exceeding the mean of that component in the ensemble by 2.5σ (standard deviation) was replaced by an average of the adjacent values. This operation was followed by a centered, three-point average applied to all interior points of each ensemble. As a final option, the profile was extrapolated from the near-bottom vector components of the ensemble to zero at the bathymetric surface (Dinehart and Burau, submitted).

The filtered velocity ensembles were imported to *Tecplot* for three-dimensional plotting of velocity vectors along each survey path. The contrast between original and filtered velocity ensembles is shown for a section of a survey path in the main channel (Fig. 4). Although the test criteria removed most outlier velocities, some remaining outliers were easily detected by visual inspection. Along a survey path, for instance, an internally uniform ensemble might vary greatly relative to adjacent ensembles because of spatial variations in local topography, and such variations were retained. However, if displayed

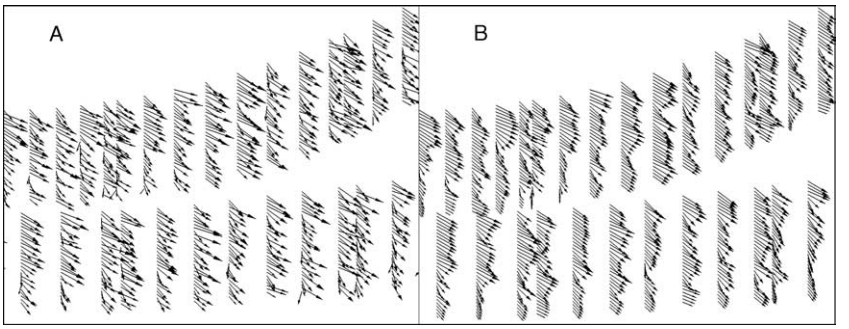

Fig. 4. Comparison of original (A) and filtered velocity ensembles (B) for an ADCP survey of Fall 2001. The filtering consisted of outlier replacement and a 3-point average for remaining vector components. Near-bed vector components were interpolated to zero at the bed elevation derived from the corrected bathymetric data.

ensembles were obvious outliers relative to adjacent ensembles over similar topography, they were considered anomalous and deleted.

To determine the effect of filtering (i.e. removing outliers and smoothing velocity ensembles), a velocity profile measured during Fall 2000 at a stationary point was analyzed. Velocity ensembles were recorded by ADCP about 1 km upstream from the study reach, at a mid-channel point. A set of velocity ensembles was collected for 5 min, with internal averaging of five ensembles before transmission every 4.7 s, about the same settings as the Fall 2000 surveys. The set of velocity ensembles was then combined into two time averages, for both unadjusted and filtered vector components.

The time averages of original and filtered horizontal velocities at all bins are shown in Fig. 5A. Velocity magnitudes of the original and filtered vector components at each bin differed by less than 2%, with an average difference over the profile of less than 0.3%. The standard deviations for sets of horizontal velocities were reduced by about 3 cm/s with filtering. Velocity magnitudes computed from filtered components of the ensembles were within 1 cm/s of velocity magnitudes filtered directly. The minimal change indicates that the time-averaged velocity profile was not biased significantly by the filtering algorithms. The time averages of original and filtered vertical velocities at all bins are shown in Fig. 5B. Because vertical velocities had fewer and smaller outliers, standard deviations of vertical vector components were reduced by less than 1 cm/s with filtering.

An unexpected finding was that some averaged profiles of vertical velocities had greater negative values within about 2 m below the ADCP. Negatively biased profiles of vertical velocities were common in spatial averages of the velocity ensembles from the Fall 2000 surveys (Fig. 5C). Spatial averages of vertical velocities from the Fall 2001 surveys had only negligible negative bias near the surface (Fig. 5D). Therefore, the flow-field interpolations for Fall 2000 were examined with caution for 3D flow directions. Instrument orientation and boat-hull interference may both contribute to the effect of negative bias, but the cause was undiagnosed in this study.

The vertical-velocity bias affected flow-field streamtraces originating near the water surface. Streamtraces calculated from origins near the water surface fell toward the middle of the flow depth more rapidly, by a factor of nearly 2, due to the increased negative vertical velocity. In the canal, which has a depth of 5 m or less, most of the measured water column was affected by the negative bias. To avoid distorted streamtrace paths, streamtrace origins were placed at least 2 m lower than the ADCP transducer elevation within vector grids in the main channel.

4.4. Backscatter intensity

While recording a velocity ensemble, ADCPs also record the acoustic intensity of signals backscattered to the device from particles suspended in the flow. The backscatter-intensity values are logged for each vertical bin along the four ADCP beams. After

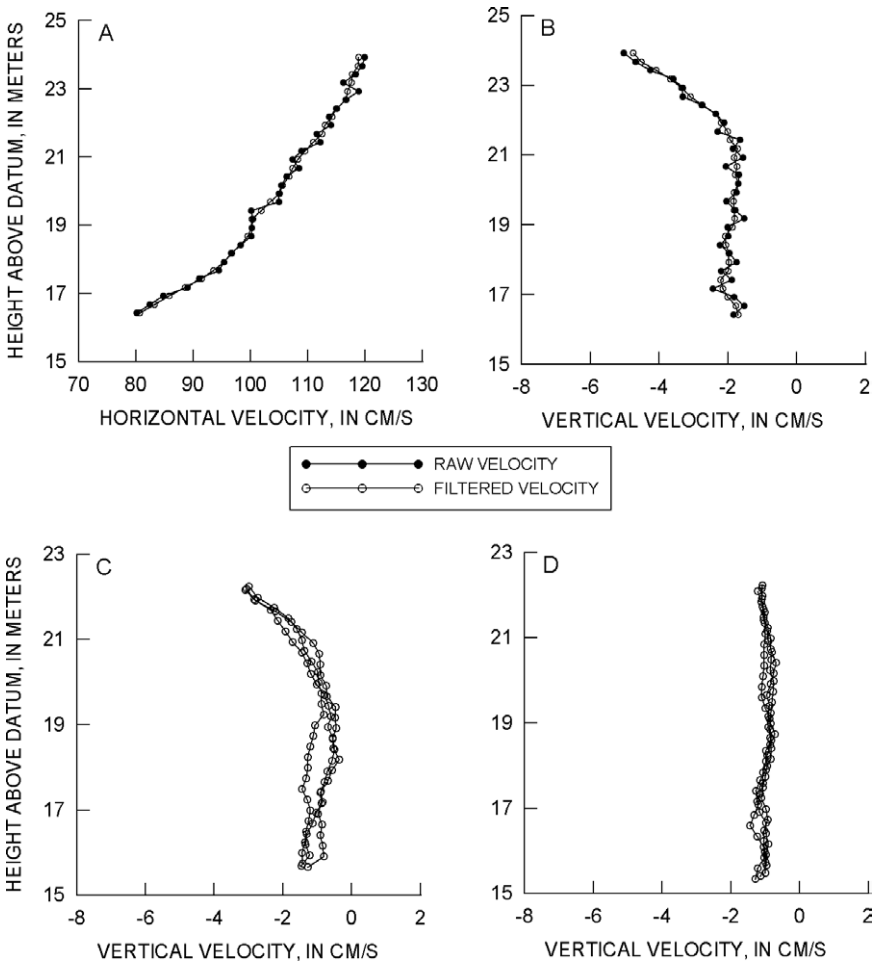

Fig. 5. Comparison of original (A) and filtered velocity ensembles (B) after time averaging of data measured at a stationary point by the concave-head ADCP. The bed elevation is at the lower axis level of 15.0 m, and the water surface is at 24.9 m. The number of samples at each bin during the time period is 89. Graphs C and D compare examples of filtered vertical velocities as measured by the concave-head ADCP (C) and convex-head ADCP (D) in the Delta Cross Channel. All profiles in C and D are spatial averages of velocity ensembles along survey paths in the main channel. The number of samples in each profile of C and D ranges from 183 to 400.

correction for depth and temperature, the vertical profile of backscatter intensity is largely a function of the concentration of suspended scatterers. However, backscatter intensity is known to be influenced by biological particles, mixing layers, and bubbles (Gordon, 1996). Therefore, the spatial distribution of backscatter intensity is not considered an exact surrogate for sediment concentration, but only an indicator. Backscatter-intensity values were extracted from the raw data files, averaged at each bin, and assigned to the corresponding positions of vector components. Outliers in vertical profiles of backscatter intensity were uncommon, and no special filtering was applied.

As with velocity ensembles, vertical profiles of backscatter intensity are not time-averaged in spatial ADCP surveys. To examine statistical properties, backscatter intensity was analyzed in the same stationary ADCP measurement of Fall 2000 in the Sacramento River. Backscatter intensity was recorded at 2.8 Hz for up to 10 min. The profile gradients were similar in all four beams, but their mean values were offset from each other at equivalent bins by 1–5 dB. The offsets were nearly linear through the usable

range (near-bed to near-surface). Standard deviation of the time series of averaged backscatter intensity ranged from 2 to 2.5 dB at mid-depth, and increased to 3 dB at the water surface and near the streambed.

As noted earlier, calibration of sediment concentration from ADCP data deserves fuller discussion, and is not included here. Several researchers have calculated in situ sediment concentration directly from backscatter intensity, or have presented physically based empirical relations between backscatter intensity and sediment concentration (Deines, 1999; Gartner, 2002).

The log of concentration of suspended scatterers (in mg/L) is considered directly proportional to the backscatter intensity (in dB) recorded by the ADCP (Deines, 1999). This relation is the basis for empirical regressions between backscatter intensity and suspended-sediment concentration. The ADCP is highly sensitive to small changes in suspended-sediment concentration, so spatial differences of several dB in backscatter intensity correspond to relatively small differences in concentration. For the low concentrations commonly measured at the study reach (20–50 mg/L), a typical increase of 10 dB in backscatter intensity corresponds to an increase in concentration by a factor of 2.

By mapping contours of backscatter intensity, an indicator for suspended-sediment concentration in the surveyed reach was obtained. Spatial maps of backscatter intensity were visualized in sequences of ADCP surveys to indicate changes in sediment distribution. By interpolating backscatter intensity to the same grids used for flow visualization, the distribution of suspended-sediment was indicated in the mapped velocity field, for possible adaptation to calculate suspended-sediment discharge.

5. Grid interpolation of flow-field data

Velocity ensembles were interpolated to 2D or 3D grids to fill the gaps between survey paths with regularly spaced vector components. Grids represented the surveyed flow field by conforming to local bathymetry and water surface. Backscatter intensity was interpolated to the same grids to visualize distribution of suspended sediment and to allow computation of backscatter flux. The flow-field data of each ADCP survey were interpolated to a separate, identical grid.

The velocity vectors and backscatter-intensity values were interpolated in *Tecplot* by an inverse-distance algorithm of the form

$$\phi_d = \frac{\sum w_s \phi_s}{\sum w_s} \tag{1}$$

where ϕ_d and ϕ_s are the variable values at the grid nodes and in the ensembles, respectively. The weighting function, w_s, was set equal to $1/D^{3.5}$, where D is the distance between the random ensemble point and the target grid point.

Velocity ensembles were processed to derive either planar or volumetric vector interpolations. For planar interpolation, three vector components u, v, w, were first vertically averaged at each navigational position. Then, the set of vertical averages for each ADCP survey was interpolated to a 2D grid. The planar interpolations reduced lateral variability in flow directions, but could not be examined for flow dynamics in much detail.

For volumetric interpolations, each set of velocity ensembles along a survey path was interpolated to a 3D grid. The i–j–k ordered grids were rectangular in x–y directions, and were extruded upward from bathymetric grids at their lower boundary. The arrangement of cells is shown in Fig. 6 for the downstream corner of a typical flow grid. Horizontal cell dimensions were scaled to resemble distances between ensembles along survey paths. Thus, x–y cells were about 4×4 m in length.

The uppermost level of nodes in each 3D grid was set to the tidal stage, with nodes spaced equally toward the bed. Vertical distances between nodes were 0.8 m, with smaller distances in the near-bed region. To maintain equal vertical spacing over irregular depths, the remaining vertical nodes were relocated to occupy the near-bed region, within 0.3 m of the lower bathymetric boundary. To compute flux at grid sections, each 3D grid was constructed with the uppermost level matching the water-surface elevation for the mean time of each survey. Alternatively, the grid could be constructed with the uppermost level of nodes at the same minimum elevation for all stages, which negated flux calculations, but allowed values at

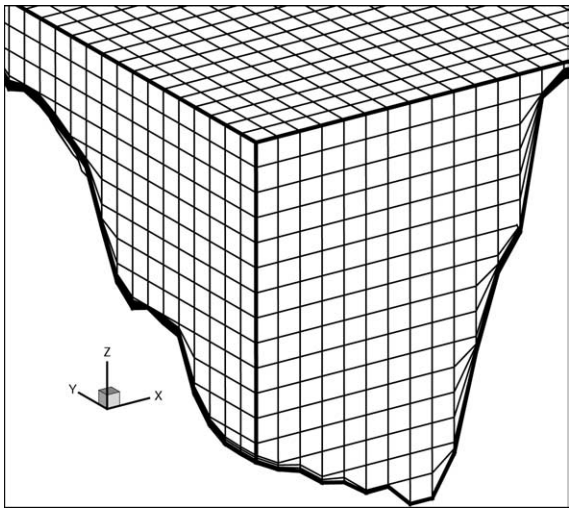

Fig. 6. The downstream corner of a 3D grid generated for the junction of Sacramento River at Delta Cross Channel. The grid conforms to bathymetry as derived from ADCP surveys. The grid is *i–j–k* ordered, with *k* corresponding to vertical levels. Additional *k*-levels are compressed near the bed to retain regular cell sizes at uniform levels in the flow field.

identical nodes to be averaged through multiple vector grids.

The average duration of an ADCP survey was limited to changes in stage less than 0.1 m (10% of range), and changes in mean velocity less than 0.1 m/s. For ADCP surveys completed within these limits, the interpolated values at vector grids were considered a synoptic represention of the flow field. As an indication of synopticity, vectors at similar lateral locations in parallel survey paths of a single survey were comparable, indicating that each ADCP survey could be treated as if collected at an identical time. During turning tide, however, velocity vectors on adjacent survey paths had rotated rapidly with respect to each other. How to survey efficiently the flow field of a channel during turning tide with an ADCP is a difficult logistical problem, as is the derivation of a representative vector grid from such a survey.

In this study, ADCP velocity ensembles were collected as described in Section 3, with five ensembles averaged before transmission for recording (Table 1). Those ensembles were further smoothed by various filtering procedures. Still, interpolated vectors of the study reach fluctuated by several degrees between adjacent nodes within the grids. These fluctuations are to be expected for single surveys through a turbulent flow field at a speed similar to flow velocity.

In an investigation of vector-interpolation methods, David et al. (2002) found that inverse-distance procedures were suited to random distributions of vector data with strong velocity gradients. The main purpose for filtering velocity ensembles was to reduce the eventual influence of outlier vector components on spatial interpolation to grid nodes. However, non-representative velocity magnitudes could also be produced by spatial interpolation from uniform velocity ensembles. Low velocities near the bank were weighted equally with high velocities near the channel center, where target grid nodes were midway between sections of the survey path. Regions of anomalously low velocity were thereby obtained in some regions near mid-channel, where the spatial density of survey paths was low. To better represent the original velocity field in an open channel, interpolation algorithms could be designed to account for velocity magnitudes along streamlines between velocity ensembles.

In this study, synopticity of ADCP data was assumed within the duration of individual surveys. For larger reaches with unsteady flows, interpolation procedures would have to account for time-dependent changes in flow during longer ADCP surveys. As used in this study, inverse-distance interpolation provided only a first approximation of velocity fields from ADCP data. Improvements in flow-interpolation procedures have been described elsewhere (Sokolov and Rintoul, 1999; Rixen and Beckers, 2002), or are available as proprietary software (Eden et al., 2000).

6. Visualization of flow and sediment dynamics

One benefit of repeating ADCP surveys along fixed paths is the time-lapse effect gained by displaying the surveys sequentially with computer animation. In these repeated surveys, one can examine tidal effects on velocity vectors and sediment suspension throughout the entire reach. However, the spatial wandering of survey paths makes displays of the flow field inconsistent from one survey to the next. The displays were improved when survey paths were interpolated

to 3D grids for animation. Animated views of the flow field were produced with vector displays or with streamtraces drawn over the corresponding bathymetric surface.

6.1. Flow dynamics

Analysis of repeated ADCP surveys through the channel junction showed how changes in tidal stage corresponded with changes in flow direction and velocity magnitudes. The sequence of flow diversion toward the canal entrance was shown with better time and spatial resolution than attainable from point measurements or parallel cross-sections. As tidal stage rises at the junction of the Sacramento River with the Delta Cross Channel, velocity slows, discharge decreases, and water enters the canal. As flow diverts from the main channel into the canal, velocity decreases downstream from the entrance. Upstream from the entrance, the velocity vectors are constantly directed seaward, and vary toward the entrance by a few degrees. Along a centerline perpendicular to the entrance, however, the vectors rotate nearly 70° during flood tide when flow is diverted to the entrance. As tide ebbs, flow returns briefly from the canal into the Sacramento River (which had not been measured previously). Changes in flow direction near the entrance are shown in selected flow-field maps of the 2001 surveys (Fig. 7).

Flow directions through the vector fields were made visible with streamtraces shown in Fig. 8a. The streamtraces simulate the paths of massless particles that follow the flow. A rake of streamtrace origins was placed near the upstream boundary of an interpolated flow field for rising tide. Before the study began, fisheries researchers thought that smolts feeding along the right bank of the main channel during rising tide would not be diverted into the canal entrance. However, streamtraces originating near the opposite bank of the main channel were shown to enter the canal for a total 4 h during each diurnal tidal cycle. The streamtrace paths derived from ADCP surveys encouraged research to observe paths of smolt migration more closely at the channel junction.

Vertical movements of massless tracers in the study reach also were visualized by placing streamtraces arbitrarily within the 3D grid. To examine the near-bed effects of flow toward the canal entrance, a rake of streamtrace origins was placed diagonally along the thalweg at a depth of 7 m in the vector grid (Fig. 8b). The streamtraces indicated a vertical movement of 5 m on paths from the thalweg into the canal entrance. The upward streamtraces could be interpreted as the movement of salmon smolt usually found in mid-channel or near the bed. If smolts are moved by the flow as massless tracers, they would likely be diverted upward and into the canal entrance during rising tide.

6.2. Sediment dynamics

ADCP backscatter intensity was analyzed as an ‘indicator’ for suspended-sediment concentration, because calibration methods are in development, and because the factors contributing to ADCP backscatter intensity are under investigation. For practical purposes, backscatter-intensity data were processed and visualized as if they were a direct function of suspended-sediment concentration. By assuming a functional relation between the two quantities, sediment dynamics can be assessed through the sequential maps of backscatter intensity.

A spatial distribution of backscatter intensity is shown in the planar contour of an ADCP survey during ebb tide (Fig. 9). The backscatter contour had repeating patterns in proximal crossings of the channel that differed by a few minutes. Assuming the patterns originated with plumes of suspended sediment, the corresponding patterns in adjacent contours indicated that sediment plumes maintained both lateral and streamwise continuity. The backscatter contours also correlated with expected sources of suspended sediment, near the depositional point bar inside the bend, and above the bedforms in the thalweg.

The cross-sectional values of backscatter-intensity rose and fell more than 20 dB through the tidal cycle, as shown by the time series for a cross-section north of the canal entrance (Fig. 10). Sequences of backscatter contours measured longitudinally at the center of the study reach indicated a reach-scale increase in backscatter intensity during ebb tide. The increase lagged the rise in mean velocity by nearly an hour. A similar lag was noted by (Kawanisi and Yokosi, 1993), where sediment concentration rose with increased longitudinal turbulence intensity that lagged

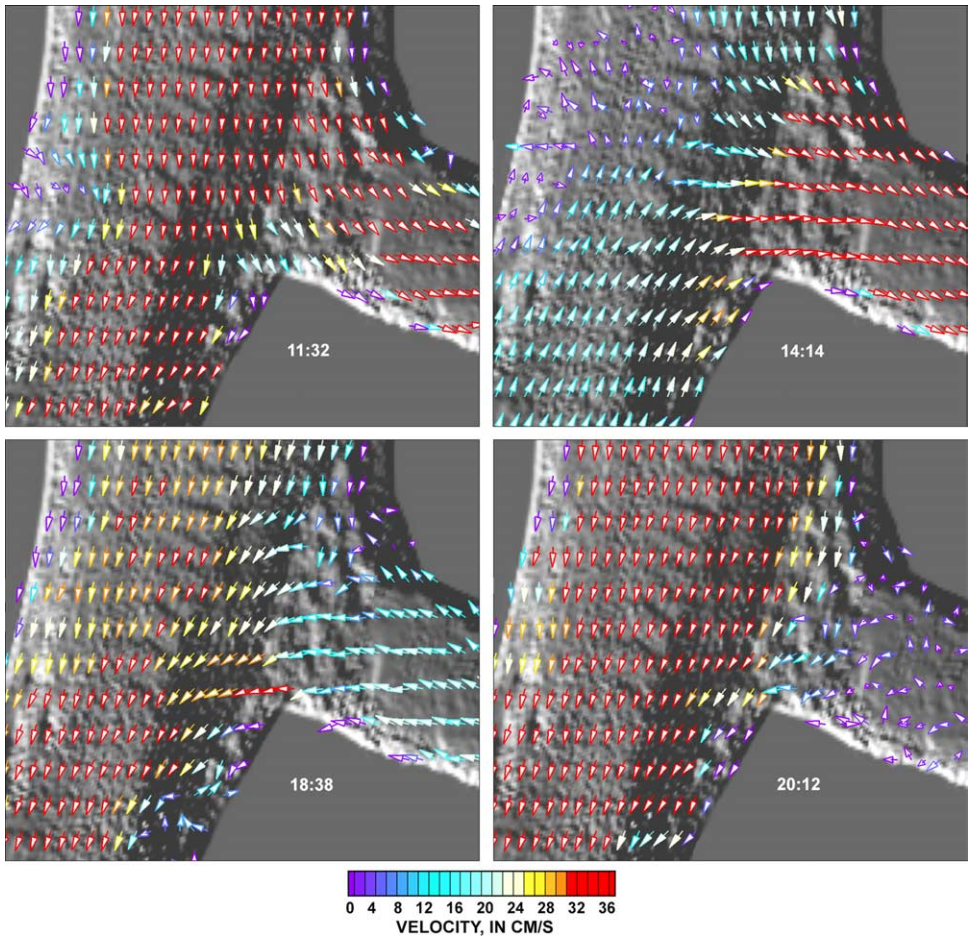

Fig. 7. Four maps of the vector field at Sacramento River at Delta Cross Channel, each determined by 2D grid interpolation from a single ADCP survey. Vertically averaged velocity is shown by uniform-length vectors with color contours for magnitude. Downstream from the canal entrance, flow direction reverses in the Sacramento River (14:14), but only slows in the main channel upstream from the canal entrance.

the rise in mean velocity. The maximum backscatter values generally coincided with high ebb velocities in the Sacramento River (Fig. 10). As velocity in the main channel decreased during flood tide, backscatter-intensity values remained higher than measured at the same velocity during ebb tide. The elevated backscatter values during decreasing velocity were most likely the effect of low settling velocity of the finer suspended sediments.

The changing distribution of backscatter intensity in the study reach corresponded with changing velocity and tidal stage. The sequences of backscatter intensity in vector grids indicated that, during ebb tide, suspended sediment migrated across the channel, and entered the canal as stage rose. As flow direction in the Sacramento River turned landward with flood tide, backscatter intensity increased in the Sacramento River at the canal entrance, indicating the transport of suspended sediment from the south into the canal for a limited period.

Flow-field interpolations of ADCP surveys were used to calculate backscatter flux as an indicator of suspended-sediment discharge through the channel junction. Suspended-sediment discharge is expressed as a mass quantity per unit time, such as tons per day for natural rivers. Calculating backscatter flux through the 3D vector grids mimics the standard computation of suspended-sediment discharge across a channel,

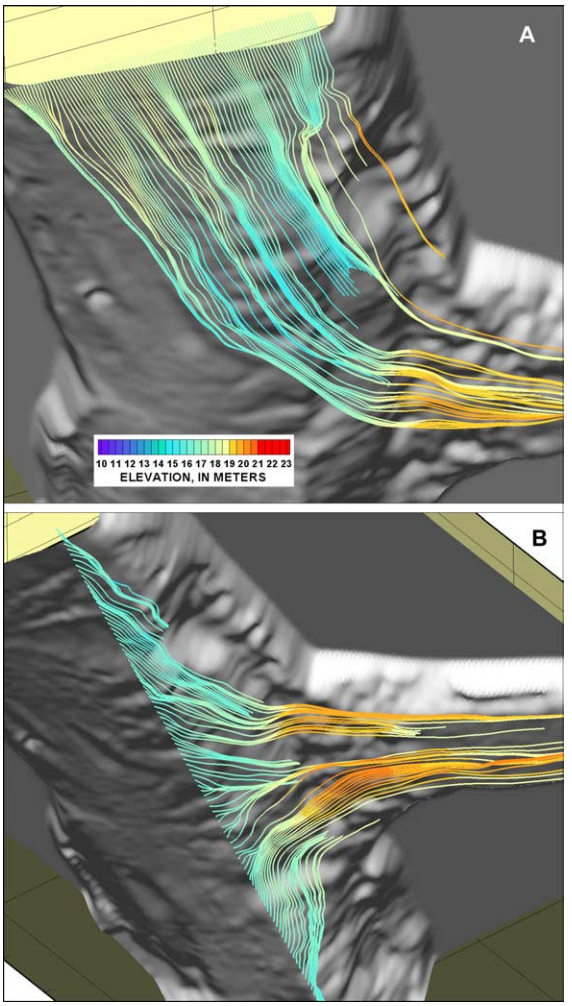

Fig. 8. Flow directions through 3D vector fields made visible with streamtraces. (A) A rake of streamtrace origins is placed at the upstream boundary of a vector field for rising tide. (B) A rake of streamtrace origins is placed diagonally along the thalweg of a vector field for rising tide. The streamtraces rise about 5 m upward into the canal entrance.

but utilizes only ADCP data. The normal vector components at cells of cross-sectional planes were multiplied by the scalar backscatter value and the resultants were integrated over the plane to obtain cross-sectional backscatter flux for each ADCP survey.

Backscatter flux was computed for two survey periods of Fall 2001 at three cross-sectional planes, at the north and south ends of the reach and in the canal (Fig. 11). The tidal-cycle total of backscatter flux for the canal and south sections is within 3% of the total backscatter flux through the north section (Table 2). The backscatter flux through the junction provided one element for computation of suspended-sediment discharge from ADCP data. The remaining element is the calibration of backscatter intensity to concentration through sediment sampling at the ADCP (Gartner, 2002). The calibrated relation would be applied to the scalar values of backscatter intensity stored with the vector arrays for each interpolated grid, followed by flux computations.

6.3. Time averages of vector grids

The visualization of individual ADCP surveys reveals the effects of macroturbulent fluctuations on the interpolated flow field. These random fluctuations can be reduced by averaging short series of velocity-vector grids. The resulting vector grid approximates the mean flow directions for the period of the chosen sequence. To obtain mean flow directions for ebb periods of the diurnal tidal cycle, time averages were computed for the appropriate sequences of 3D vector grids.

The time average of a long series of vector grids can be approximated as,

$$A[v(t)] = \frac{1}{2T}\int_{-T}^{T} v(t)\,\mathrm{d}t \tag{2}$$

where $v(t)$ is an array of vectors and T is a finite time.

For a finite series of vector grids derived from ADCP surveys, the integral of $v(t)$ is derived from the trapezoidal rule for integration of unequal segments. For each of the three vector components, the time average of $v(t)$ takes the form,

$$A[v(t)] = \frac{1}{(t_n - t_0)}\left(h_1\frac{v(t_0)+v(t_1)}{2} + h_2\frac{v(t_1)+v(t_2)}{2} + \cdots + h_n\frac{v(t_{n-1})+v(t_n)}{2}\right) \tag{3}$$

where h_n is the time interval between the mean survey times of two measurements, t_{n-1} and t_n, and $v(t_n)$ is the array of vectors for a grid at any time t_n. Velocities

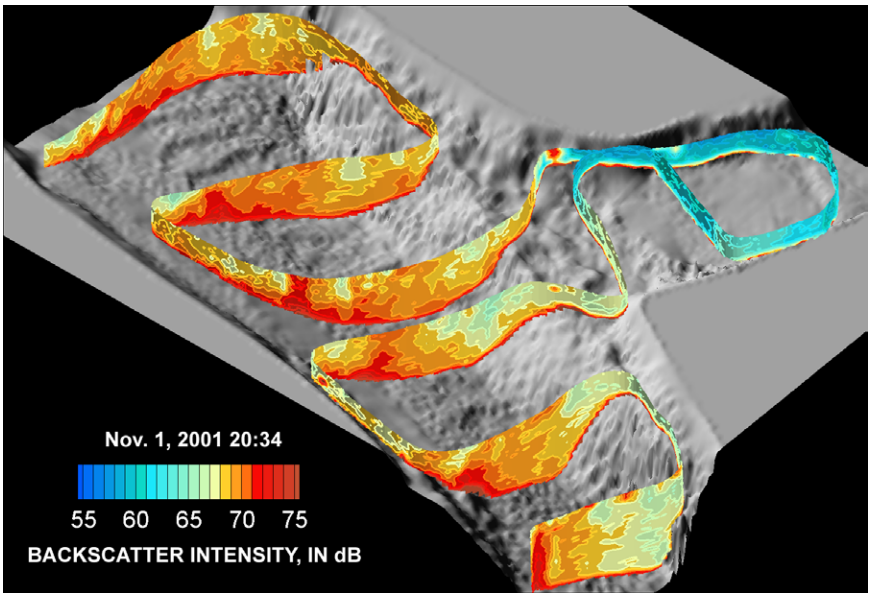

Fig. 9. A planar contour of backscatter intensity shown along a survey path, Fall 2001. Patterns show correspondence in adjacent crossings. Higher backscatter values occur across the depositional bar (at left in figure, along bank). Flow is seaward in main channel, with minimal diversion to canal.

were averaged at identical nodes for the series of vector grids.

From only a few ADCP surveys, a plausible map of three-dimensional flow in the reach can be derived. To obtain a vector grid of mean flow directions in the main channel, eight vector grids were time averaged (Eq. 3) over an ebb period during a Fall 2001 survey when little flow was diverted to the canal. Streamtrace origins were set at the upstream end of the time-averaged vector grid, at 4 m below the surface (Fig. 12). Secondary circulation in the bend produced the falling elevation of streamtraces that trend toward the west bank (Dinehart and Burau, submitted). An enlarged view of the enclosed area on Fig. 12 shows the averaged velocity ensembles in plan view (Fig. 13). The velocity ensembles have near-bed vectors that are rotated west at 10–30° with respect to the near-surface vectors.

By time-averaging vector grids over one diurnal tidal cycle, a spatial map of backscatter intensity

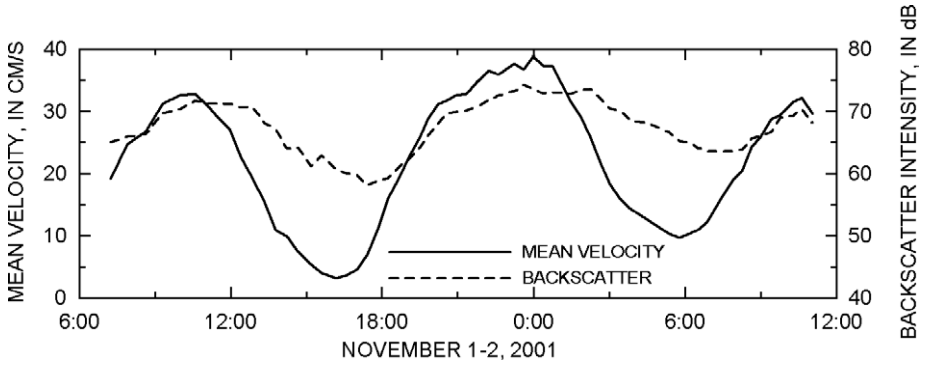

Fig. 10. Line plots of mean velocity and mean backscatter intensity are shown for a cross-section near the upstream end of the vector grid, Fall 2001. The minimum backscatter intensity lags minimum velocity by more than 1 h.

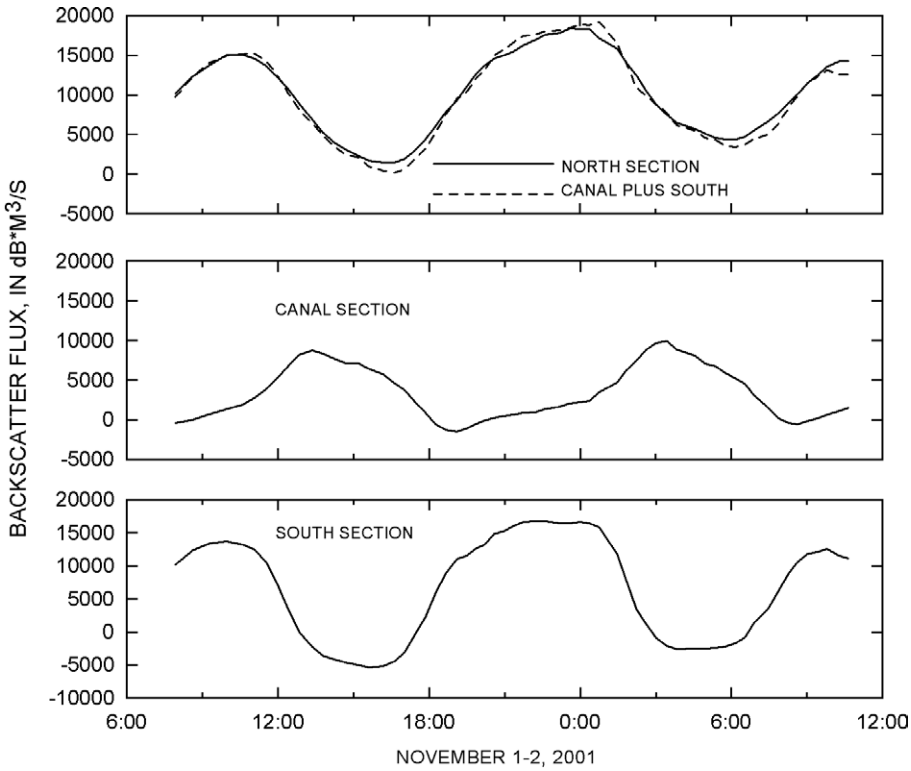

Fig. 11. Backscatter flux (product of backscatter intensity and velocity normal to the plane) is shown in line plots for the upstream end of the vector grid (North Section), the west end of the canal (Canal Section), and the downstream end of the grid (South Section). The dashed line shows the sum of backscatter flux at the Canal and South Sections.

was derived (Fig. 14). Contrasted with the erratic deviations of single backscatter surveys, the time-averaged distribution of backscatter intensity varied uniformly across the channel, with greater values measured near the streambed and in the reach seaward from the canal entrance. Although the spatial map of backscatter intensity represents no single condition of the surveyed reach, it indicates regions of the channel dominated by suspended sediment.

7. Technical refinements

Although spatial mapping of flow fields with ADCPs has become routine in shallow ports and waterways, its application in riverine channels was still uncommon during this study (2001). By visualizing ADCP data from multiple surveys with various approaches, we were able to refine velocity-mapping strategies for large rivers. The distances between survey paths (>30 m) in the study area produced uncertainty in vector directions when interpolated to grids by inverse-distance procedures. Velocity profiles lacked resolution near the streambed because of inherent ADCP limitations. However, reduction of these

Table 2
Two examples of backscatter-flux computations for three cross-sections in junction of Sacramento River with Delta Cross Channel, Fall 2001

Total backscatter flux at sections	6:18 Oct. 29–11:39 Oct. 30	7:14 Nov. 1–11:01 Nov. 2
North	540,000	618,000
Canal	169,000	203,000
South	361,000	396,000
Canal + South	530,000	599,000

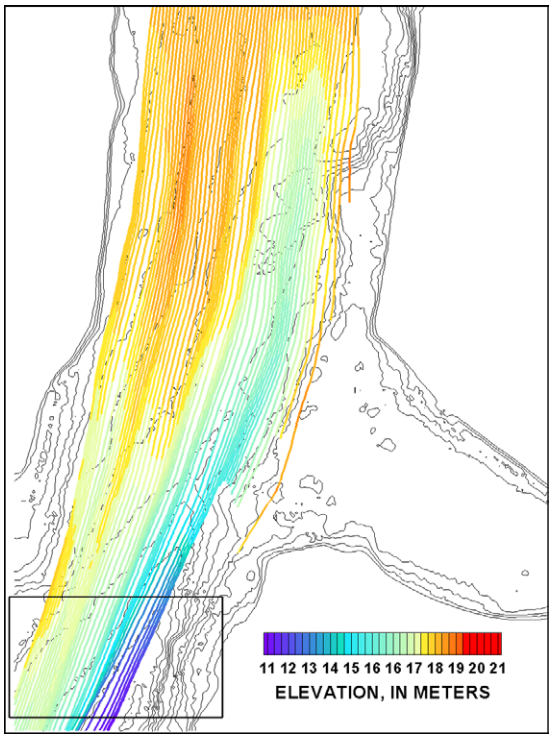

Fig. 12. Streamtraces through a time-averaged 3D vector field, determined from a sequence of seven ADCP surveys during ebb tide (Fall 2001). A rake of streamtrace origins is placed at the upstream boundary of the vector field. The decrease in streamtrace elevation shows the effect of secondary circulation at the south end of the study reach. The enclosed area is enlarged for vector components in Fig. 13. (Bathymetric contour interval, 1 m.)

uncertainties will become a priority for incremental improvements in channel flow mapping.

Velocity fields of free-surface flows have been measured with high spatial resolution at limited depths or in laboratory cross-sections (Smith, 2002; Blanckaert, 2002). When repeated ADCP surveys are applied over large reaches of tidal rivers, uncertainty in the velocity field increases. The uncertainty can be reduced by deploying multiple ADCPs on multiple vessels, by choosing sampling modes appropriate to the velocity scales of interest, or by making the survey-path network denser at a similar time duration. For small channel reaches in steady flow, the uncertainty is easily reduced by repeating single cross-sectional surveys rapidly and then time-averaging sets of interpolated surveys. Other large channel junctions in the Sacramento-San Joaquin River Delta have been investigated successfully with repeated ADCP surveys (Burau et al., 2003b; Cuetara et al., 2003). Surveys of larger junctions at a reliable time resolution are more difficult to obtain, but still provide useful data on hydraulic relations between tributaries.

8. Summary

To evaluate effects of the Delta Cross Channel on migrating salmon smolts, 3D vector grids were

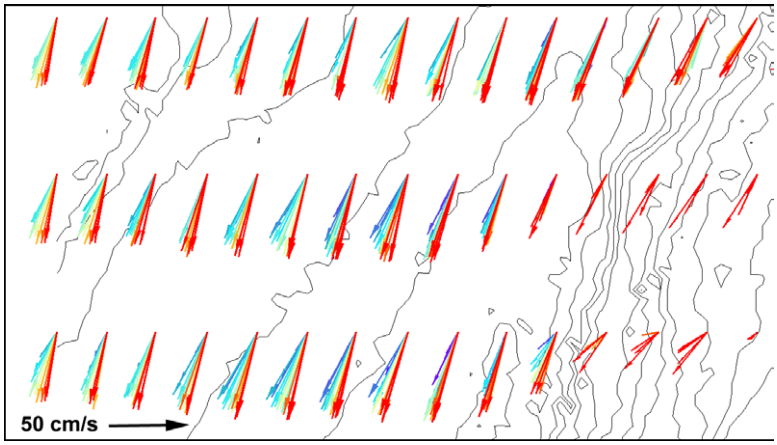

Fig. 13. Velocity ensembles of the time-averaged 3D vector field shown in plan view for the enclosed area of Fig. 12. A subset of east–west planes is displayed. The velocity ensembles have near-bed vectors that are rotated west at 10–30° with respect to the near-surface vectors.

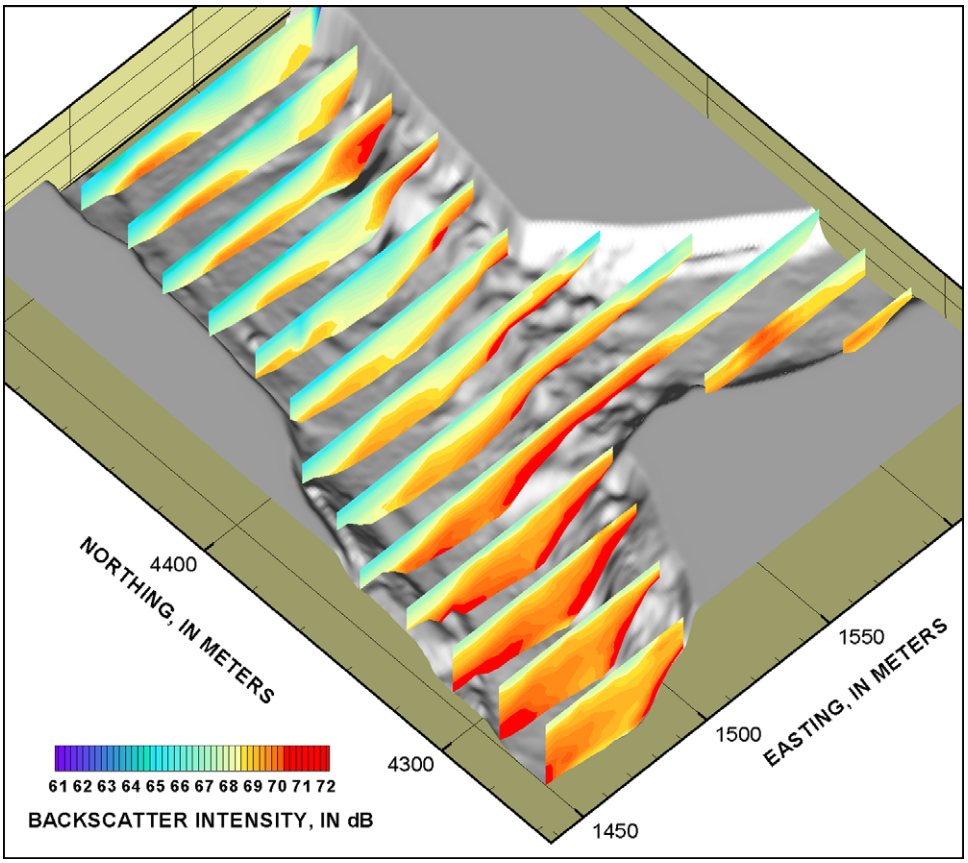

Fig. 14. Backscatter intensity derived by time-averaging vector grids to a final grid over one diurnal tidal cycle (Fall 2001). A subset of east–west planes is displayed.

created from repeated ADCP surveys in the channel junction at the Sacramento River. Batch processing of ADCP output files was essential for efficient spatial analysis of the multiple surveys. Systematic and random errors in the ADCP data were corrected through a series of automatic routines and user interventions. Accurate bathymetry that was concurrent with velocity measurements was obtained from the individual ADCP beam depths, and was used as the base for 3D vector grids. Backscatter intensity was mapped and analyzed as an indicator of suspended sediment, and formed a basis for future computations of suspended-sediment discharge.

By interpolating the ADCP surveys to 3D vector grids, flow and sediment dynamics in the channel junction were visualized over diurnal tidal cycles, using only ADCP data. Streamtraces indicated the range of diversion of salmon smolts from the main channel into the canal entrance. The interpolated velocity fields were investigated for velocity magnitudes and directions through the entire tidal cycle. Although inverse-distance interpolation was readily acknowledged to provide only a first approximation of velocity fields from ADCP data, the potential value of more sophisticated interpolation is apparent. The spatial analyses of ADCP data show that a strategy of repeated surveys and flow-field interpolation has the potential to simplify computation of flow and sediment discharge through complex waterways.

Acknowledgements

The ADCP survey data for the study reach were collected by the San Francisco Bay-Delta Hydrodynamics Project of the USGS. Jay Cuetara and Jon Yokomizo were the primary pilots during ADCP surveys. Michael Simpson generously advised us on interpretation of ADCP data. This research was supported by projects of the CalFed Bay-Delta Authority, *Sedimentation in the Delta* and *Delta Cross Channel Gate Operations*, and was approved by the USGS on January 19, 2004, for publication. Thoughtful colleague reviews were provided by Roger Denlinger, USGS, Vancouver, and Peter E. Smith, USGS, Sacramento, which helped to improve and clarify the discussion.

Appendix

Transformations are described here to calculate geographic coordinates of beam-contact positions from depths recorded by ADCPs (RD Instruments). The ADCP measures a separate distance to the streambed along each of four transducer beams. The distances to streambed along the 20-degree inclination from vertical are converted to four vertical depths and recorded by the RD Instruments software, *WinRiver*. Each depth includes the draft of the ADCP below water surface. For distance conversions, the *x*–*y* coordinates of each beam contact are calculated with no correction for pitch or roll:

$X(1) = -\mathrm{Raw}(1)^{*} \tan\theta^{*} \mathrm{face}$
$X(2) = \mathrm{Raw}(2)^{*} \tan\theta^{*} \mathrm{face}$
$X(3) = 0$
$X(4) = 0$
$Y(1) = 0$
$Y(2) = 0$
$Y(3) = \mathrm{Raw}(3)^{*} \tan\theta^{*} \mathrm{face}$
$Y(4) = -\mathrm{Raw}(4)^{*} \tan\theta^{*} \mathrm{face}$

where Raw(n) are the four recorded vertical depths for the same-numbered transducers, with Draft subtracted; *face* is 1 for convex and (−1) for concave arrangements; and θ is the transducer angle measured from vertical. The y-axis is assumed parallel with the vessel center line (bow to stern), according to marine convention. To apply measured pitch and roll, the coordinates are rotated through their axes by:

$$\bar{X} = X\cos\alpha + Y\sin\alpha$$

$$\bar{Y} = -X\sin\alpha + Y\cos\alpha$$

A rotation of the ADCP beams along the pitch axis affects only the Y and Z coordinates for beam-contact coordinates of each transducer n:

$$Y'(n) = Y(n)\cos\phi + \mathrm{Raw}(n)\sin\phi$$

$$Z'(n) = -Y(n)\sin\phi + \mathrm{Raw}(n)\cos\phi$$

where primes indicate rotated coordinates, and ϕ is the pitch angle.

The ADCP records a positive roll angle as it rolls counterclockwise. The ADCP beams are rotated by the roll angle around the pitch axis to obtain the new coordinates:

$$X'(n) = X(n)\cos\rho + Z'(n)\sin\rho$$

$$Z''(n) = -X(n)\sin\rho + Z'(n)\cos\rho$$

where double primes indicate a second rotation of coordinates, and ρ is the roll angle. After pitch and roll adjustments, the coordinates are rotated according to the compass heading by:

$$X''(n) = X'(n)\cos\gamma + Y'(n)\sin\gamma$$

$$Y''(n) = -X'(n)\sin\gamma + Y'(n)\cos\gamma$$

where γ is the heading in radians. The ADCP draft is then added to each depth:

$$Z''(n) = Z''(n) + \mathrm{Draft}$$

Finally, the rotated local coordinates $X''(n)$, $Y''(n)$ are added to the geographic coordinates of the ADCP center as recorded by GPS, with the elevation coordinate determined by subtraction of $Z''(n)$ from local water-surface elevation.

References

Blanckaert, K., 2002. Analysis of coherent flow structures in a bend based on instantaneous-velocity profiling, Proceedings of Third International Symposium on Ultrasonic Doppler Methods for Fluid Mechanics and Fluid Engineering, EPFL, Lausanne, Switzerland 2002 pp. 51–58.

Burau, J.R., Cuetara, J.I., Ruhl, C.A., George, J.E., 2003a. Hydrodynamics of the Delta Cross Channel region, Proceedings of the CalFed Bay-Delta Program Science Conference, Sacramento, California 2003 p. 19.

Burau, J.R., Cuetara, J.I., Ruhl, C.A., Dinehart, R.L., George, J.E., 2003b. Effects of the tides, geometry, meteorology, and project operations on circulation and mixing in a flooded island environment: Lessons from Mildred Island, Proceedings of the CalFed Bay-Delta Program Science Conference, Sacramento, California 2003 p. 20.

Cuetara, J.I., Burau, J.R., Ruhl, C.A., Simpson, M.R., Dinehart, R.L., George, J.E., 2003. Hydrodynamic field investigation on the San Joaquin River near the head of Old River barrier, Proceedings of the CalFed Bay-Delta Program Science Conference, Sacramento, California 2003 p. 31.

David, Laurent, Esnault, Aurelie, Callaud, T.D., 2002. Comparison of interpolation techniques for 2D and 3D velocimetry, Eleventh International Symposium on Application of Laser Techniques to Fluid Mechanics, Lisbon, July 8–11, 2002, 8 pp.

Deines, K.L., 1999. Backscatter estimation using broadband acoustic Doppler current profilers, Proceedings of the IEEE Sixth Working Conference on Current Measurements, San Diego, CA 1999 pp. 249–253.

De Serres, B., Roy, A.G., Biron, P.M., Best, J.L., 1999. Three dimensional flow structure at a river channel confluence with discordant beds. Geomorphology 26, 313–335.

Dinehart, R.L., 2000. Bedform movement in Three Mile Slough near San Joaquin River, Proceedings of the CalFed Bay-Delta Program Science Conference, Sacramento, California 2000 p. 234.

Dinehart, R.L., 2003. Spatial analysis of ADCP data in streams, Proceedings of the workshop, Sediment Monitoring Instrument and Analysis Research, Flagstaff, AZ 2003 p. 8.

Dinehart, R.L., Burau, J.R., submitted. Averaged indicators of secondary flow in repeated ADCP crossings of bends, submitted to Water Resources Research.

Eden, H., Muller, V., Vorrath, D., 2000. A hydrodynamic information-system for dynamic sediment transport, Proceedings of Hydrographentag 2000, German Hydrographic Society, Bremerhaven, Germany 2000 p. 4.

Gartner, J.W., 2002. Estimation of suspended solids concentrations based on acoustic backscatter intensity: Theoretical background, paper presented at Turbidity and Other Sediment Surrogates Workshop, April 30–May 2, 2002, Reno, NV., 4 pp.

Gordon, L., 1996. Acoustic Doppler current profiler-Principles of operation: A practical primer, Second ed., RD Instruments 1996 p. 41.

Hanson, C.H., 1996. Georgiana Slough acoustic barrier applied research project: results of 1994 phase II field tests, Interagency Ecological Program, Technical Report 44, p. 86.

Horn, M.J., 2003. Delta Cross-Channel hydrodynamics and the potential for entrainment of outmigrating juvenile salmon, Proceedings of the CalFed Bay-Delta Program Science Conference, Sacramento, California 2003 p. 82.

Kawanisi, K., Yokosi, S., 1993. Measurements of turbulence and suspended sediment in tidal river. Journal of Hydraulic Engineering 119 (6), 704–724.

Kjelson, M.A., Greene, S., Brandes, P., 1999. A model for estimating mortality and survival of fall-run Chinook salmon smolts in the Sacramento River delta between Sacramento and Chipps Island, USFWS, Stockton, CA 1999.

Lane, S.N., Biron, P.M., Bradbrook, K.F., Butler, J.B., Chandler, J.H., Crowell, M.D., McLelland, S.J., Richards, K.S., Roy, A.G., 1998. Three-dimensional measurements of river channel flow processes using acoustic Doppler velocimetry. Earth Surface Processes and Landforms 23 (13), 1247–1267.

Matthews, P., 1997. The impact of nonsynoptic sampling on mesoscale oceanographic surveys with towed instruments. Journal of Physical Oceanography 14, 162–174.

Nezu, I., Tominaga, A., Nakagawa, H., 1993. Field measurements of secondary currents in straight rivers. Journal of Hydraulic Engineering 119 (5), 598–614.

Rhoads, B.L., Kenworthy, S.T., 1995. Flow structure at an asymmetrical stream confluence. Geomorphology 11, 273–293.

Rixen, M., Beckers, J.M., 2002. A synopticity test of a sampling pattern in the Alboran Sea. Journal of Marine Systems 35, 111–130.

Simpson, M.R., Bland, R., 2000. Methods for accurate estimation of net discharge in a tidal channel. IEEE Journal of Oceanic Engineering 25 (4), 437–445.

Simpson, M.R., 2001. Discharge measurements using a broad-band acoustic Doppler current profiler, US Geol. Survey Open-file Report 01-1, at http://pubs.water.usgs.gov/ofr0101.

Simpson, M.R., Oltmann, R.N., 1993. Discharge-measurement system using an acoustic Doppler current profiler with application to large rivers and estuaries, US Geol. Survey Water-Supply Paper 2395.

Smith, J.A., 2002. On the use of phased-array Doppler sonars near shore. Journal of Atmospheric and Oceanic Technology 19 (5), 725–737.

Sokolov, S., Rintoul, S., 1999. Some remarks on interpolation of nonstationary oceanographic fields. Journal of Atmospheric and Oceanic Technology 16, 1434–1449.

Sukhodolov, A., Thiele, M., Bungartz, H., 1998. Turbulence structure in a river reach with sand bed. Water Resources Research 34 (5), 1317–1334.

US Fish and Wildlife Service, 1992. Measures to improve the protection of Chinook salmon in the Sacramento/San Joaquin River delta. WRINT-USFWS-7. Submitted to the State Water Resources Control Board, July 6, 1992.